



Structural behavior of Lightweight and High strength Layered Hollow Core Slabs

Louay A. Aboul-Nour, Ahmed S. Eisa, Asmaa El-Ghamry

University of Zagazig, Egypt

louayabdelrakek@yahoo.com

ahmedeisa@zu.edu.eg, <http://orcid.org/0000-0002-6606-3253>

f_ghamry@yahoo.com

ABSTRACT. A new technique of Layered Hollow Core Slab (LHCS) has been used to obtain a slab with an optimum weight-to-strength ratio. Specimens with a 90 mm top layer of High Strength Concrete (HSC) and a 90 mm bottom layer of Lightweight Aggregate Concrete (LWAC) were examined. Nine full-scale slabs with dimensions of 1600* 450* 180 mm were tested under a 4-point loading test. The %core, a/d, RFT ratio, and connection method were the different studied parameters. A push-out test was conducted on triplet specimens to study the bond strength at the interface between HSC jacket and LWAC cubes using bond agent material or shear dowels, or without treatment, to determine which method of them is suitable for connecting the two layers of the tested slabs. Load, deflection, ductility, strain, crack pattern, and mode of failure were studied. The results indicate that ultimate strength is enhanced with decreasing a/d and %core and with an increasing RFT ratio of the LHCS specimens. Using shear dowels ensures an efficient bond between the two layers of the tested slabs. ANSYS program used for modelling the slab. The numerical study accepted the experimental data with a variation of less than 10% for all slabs.

KEYWORDS. Hollow core slab, Layered slab, Lightweight aggregate concrete, High strength concrete.



Citation: Aboul-Nour, L. A., Eisa, A. S., El-Ghamry, A., Structural behavior of Lightweight and High strength Layered Hollow Core Slabs, *Frattura ed Integrità Strutturale*, 63 (2023) 134-152.

Received: 07.09.2022

Accepted: 27.10.2022

Online first: 15.11.2022

Published: 01.01.2023

Copyright: © 2023 This is an open access article under the terms of the CC-BY 4.0, which permits unrestricted use, distribution, and reproduction in any medium, provided the original author and source are credited.

INTRODUCTION

A hollow core slab (HCS) is defined as a simply supported concrete slab with about (40%–50%) voids in the center of the slab cross section through its length in one direction with a typical diameter of (.667-.75) of the slab thickness, a typical width of 120 cm, a typical thickness of about (15–50) cm, and the clear span reaches up to 18m [1–4]. There are many advantages of using HCS, like reducing overall weight, saving cost and time of construction, providing long spans, and increasing fire resistance [5–8]. The shear span to effective depth (a/d) ratio affects the mode of failure of the HCS and changes it from a flexural to a shear mode [9]. The ultimate load decreases with increasing the deflection when increasing the



ratio of (a/d) [10]. Increasing the core diameter of HCS caused a decrease in the ultimate load and an increase in the deflection [4]. Couplet and triplet specimens were used to study the shear and tensile bond strengths of specimens with different treatment methods, and it could be concluded that the composite action could be attained with a shear bond strength of 1 MPa at least in the semi-precast HCS and overtopping layer. The ultimate load and deflection for HCS treated with bond agent materials and shear keys increased compared to slabs without treatment [11]. Push-off tests were carried out on (40 x 40) cm of topping slab with a typical value of the shear strength at the interface of about 0.19 MPa [12]. Juozas Masenas et al. [13] investigated an experimental and numerical study on the deflection of the layered concrete slab with plastic inserts. It was found that the slab performance is highly affected by the shear stiffness of the bond between the two concrete layers, and the slab collapses when the bond is damaged and the layers slip in the support region. Increasing the a/d ratio leads to decreasing the peak load of the uncracked HCS and decreasing its peak displacement. Also, using shear keys to connect a bonded overlay concrete layer to a pre-cracked HCS leads to increasing peak load and decreasing peak displacement [14]. Using steel anchors for connecting the topping concrete layer to precast prestressed HCS decreased the deflection and increased moment capacities and stiffness as it avoids slippage. Also, using full-span steel anchors caused a full composite action better than shear span [15].

Layered elements can be cast in two ways: fresh-on-fresh and fresh-on-hardened casting methods. The fresh-on-fresh casting method is classified into two groups: horizontal and vertical layers [16]. Layered concrete has many advantages, such as: saving construction time; saving overall cost; reducing cement consumption; having a high strength to overall weight ratio; and having good impact; thermal, and durability properties [17–21]. Utilizing alternative binders to replace cement in graded concrete with using lightweight concrete to reduce the overall weight can preserve the cement consumption and reduce the construction cost up to 50% [22–26]. Using normal strength concrete for satisfying required ductility in the compression zone and lightweight concrete for reducing overall weight in the tensile zone of the layered element shows good results, and no bond problems between concrete layers have been investigated [27]. Bonding strength between concrete layers is influenced by three issues: the use of reinforcements, friction between layers, and natural adhesion [28]. The interface between concrete layers can be displayed with 3 layers: the contact layer, the overlay, and the substrate [29]. Concrete-to-concrete bonding strength is affected by different factors such as: compaction technique, substrate surface state, curing procedure, usage of bonding agents, age of chemical bonds, and mechanical characteristics of concrete [29]. Roughening the interface between concrete layers increases its bond strength [30]. The use of shear connectors to connect the normal strength concrete layer with the high strength concrete layer improved the flexural and bond strength [31]. The two-layered beam showed excellent flexural strength with a strong bond at the interface [32]. The two-layered slabs have advantages regarding the rigidity or bending of the slab, as they display 10% fewer deflections than the one-layered slab. Using the two-layered slabs gives a higher level of crack resistance [33]. The flexural strength, deflection, and failure mode of the layered section are enhanced compared with the single-layered LWAC beam and slightly affected compared with the single-layered NC beam [21]. The deflection and compressive strain have been decreased for two-layered beams compared to single-layered [34]. Ductility and load-bearing capacity of layered beams have been improved compared with single-layered beams [35].

High strength concrete (HSC) with high compressive strength, high density, and low permeability can be produced by replacing cement with binder admixture such as silica fume [36–38]. The water to binder ratio of the HSC should be kept low [38]. Using super-plasticizers for HSC mixes reduced its needed water. The optimal quantity of whole binder materials in HSC is within the range of (450 to 550) Kg/m³ [38]. Applying HSC in the compression zone of a layered element is required to resist higher bending moments while taking into account the economic benefits of higher strength[39].

Lightweight concrete (LWC) with a cylinder compressive strength of more than 41 MP is considered a HSC [2].

Expanded Perlite Aggregate (EPA) is a manufactured Lightweight Aggregate (LWA) used for producing Lightweight Aggregate Concrete (LWAC) [40]. A concrete with a density of not more than 2000 kg/m³ and a compressive strength of more than 18 MPa is considered a LWAC [41]. Applying LWAC to produce HCS elements contributes to enhancing thermal insulation, preserving natural lightweight aggregates, saving construction costs, and decreasing environmental pollution [41]. When compared to a single-layered beam, a lightweight concrete two-layered beam reduced its own weight by 34%[42].

In this study, Layered Hollow Core Slab system has been used to obtain a slab with an optimum weight-to-strength ratio.

EXPERIMENTAL PROGRAM AND SETUP

The experimental study has been done in two steps: firstly, the mechanical properties of the used two concrete mixtures have been studied; secondly, the structural behavior of the layered hollow core slabs has been investigated.



Test specimens

Compressive strength [fcu] at age of curing of 28-days on cubes (100) mm³, splitting-tensile strength [fsp] on cylinders (100 * 200) mm, flexural strength [fr] on prisms (100*100*500) mm have been carried out to determine the mechanical properties of concrete mixes. A push-out test on triplet specimens has been done to study the shear bond strength [fb] between the two concrete layers (LWAC and HSC) with different connection methods (Fig. 1). Nine LHCS specimens were examined by considering four different variables (Tab. 1). Fig. 2 shows the slab dimensions and cross section.

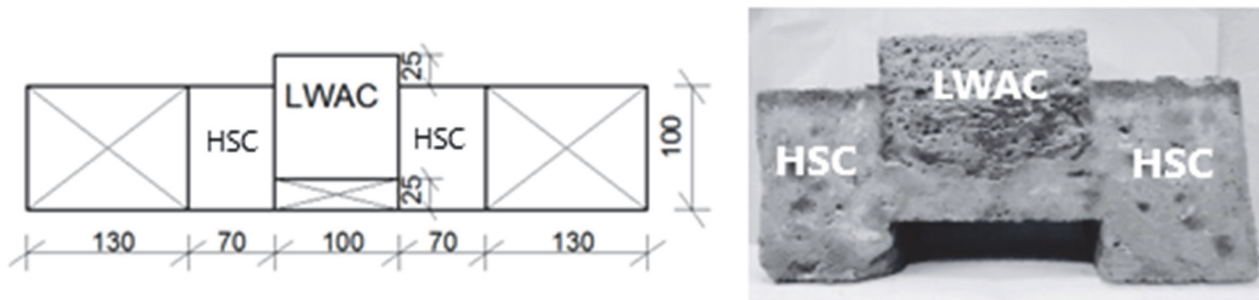
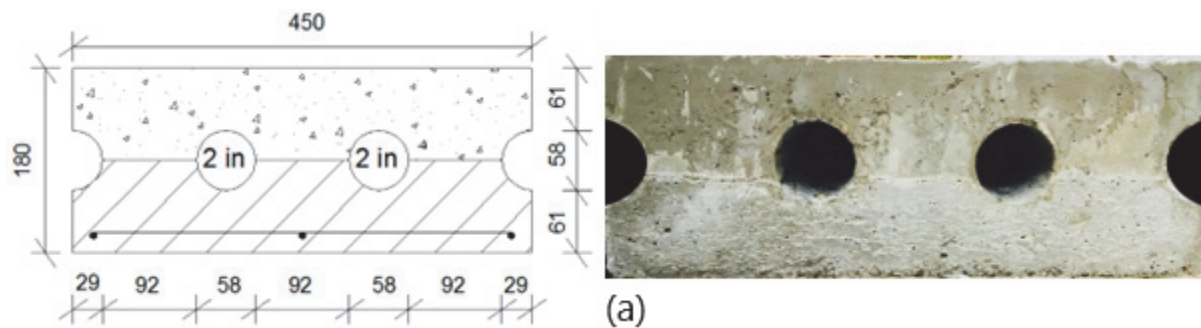


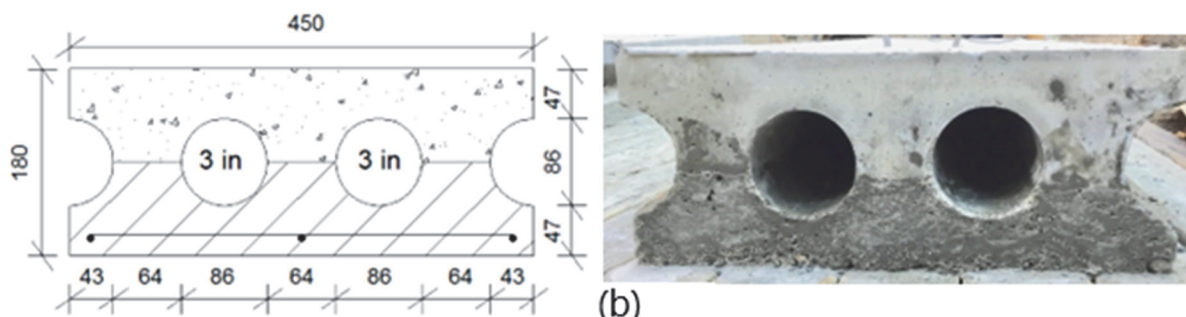
Figure 1: Triplet specimen for push-out test for bond strength.

Slab no.	LHCS 1	LHCS 2	LHCS 3	LHCS 4	LHCS 5	LHCS 6	LHCS 7	LHCS 8	LHCS 9
% Core	21.5	35.2	9.785	21.5	21.5	21.5	21.5	21.5	21.5
a/d	4	4	4	4	4	1	2.5	1	4
As	3Φ12	3Φ12	3Φ12	3Φ10	3Φ16	3Φ12	3Φ12	3Φ12	3Φ12
Conn. method	Bond agent	dowels	dowels						

Table 1: Test specimen.



(a)



(b)

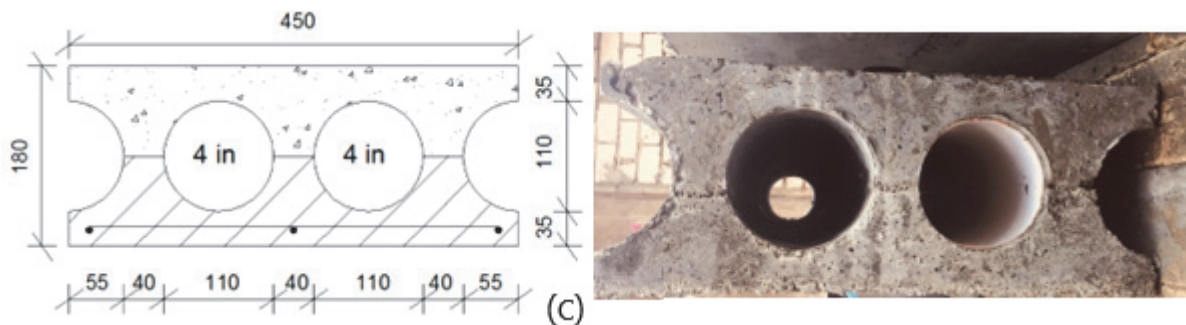


Figure 2: Slab dimensions and cross sections (mm): (a) %core=9.785%, (b) %core=21.5%, and (c) %core=35.2%.

Materials and concrete mix

The procedure of the LWAC and HSC mix used in this study is based on the previous study [43] given in Tab. 2.

Concrete: Ordinary Portland cement (OPC) type I, chemical admixture (super-plasticizer), silica fume, mixing water, gravel, sand, and Expanded Perlite Aggregate were mixed as given in Tab. 2 to obtain LWAC and HSC concrete mixtures with mechanical properties as given in Tab. 3.

Steel Reinforcement (RFT): The LHCS specimens were reinforced with a bottom net steel reinforcement with a main RFT of (10, or 12, or 16) mm high-strength deformed steel bars and a secondary RFT of (10) mm bars. 8mm plain steel bars were used for shear dowels to connect the two concrete layers. The properties of the used steel are given in Tab. 4.

Bond agent material: Addibond-65 slurry has been used for bonding fresh concrete (HSC layer) to old concrete (LWAC layer) of the LHCS specimens. The properties of Addibond-65 are given in Tab. 5.

Mix no.	EPA%	w/b	Cement	Silica fume	Super plasticizer	Water	Sand	Gravel	Perlite
Mix (1) LWAC	40	.40	520	78	24	240	161.7	194.08	129.4
Mix (2) HSC	0	.25	520	78	24	149.5	553.24	1106.48	0

Table 2: Concrete mix design (kg/m^3) [43].

Mix no.	Fcu 28-days (MPa)	Fsp (MPa)	Fr (MPa)	$\rho(\text{kg}/\text{m}^3)$
Mix (1) LWAC	21.8	1.28	2.19	1526
Mix (2) HSC	62.5	4.53	5.73	2594

Table 3: Mechanical properties of the two used mixes (LWAC & HSC).

Bar diameter (mm)	Bar type	Yield strength Fy (MPa)	Tensile strength Fu (MPa)	Modulus of elasticity (GPa)	Elongation %
8	Plain	400	450	200	22
10, 12, 16	Deformed	525	620	200	13

Table 4: Details of used steel reinforcement.

Property	Compressive strength (kg/cm^2)	Tensile strength (kg/cm^2)	Bending strength (kg/cm^2)	Abrasion resistance % loss	%Water absorption	Chemical resistance 5% H ₂ SO ₄	(%) at change 7 days) Kerosen
value	168	12	28	4.2	9.65	8	4.8

Table 5: Properties of bond agent material (addibond-65) [44].

Molding, mix proportion, casting and curing procedure

For triplet specimens, the LWAC cube (100*100*100) mm with a compressive strength of 21.8 MPa has been cast. 24 hrs later, the two HSC jackets (100*100*70) mm with a compressive strength of 62.5 MPa have been cast on the two opposite



faces of the prepared LWAC cube. Triplet specimens with shear dowels prepared with steel bar with a diameter of 8 mm with a fixed length of 3 cm in the LWAC cube from the two sides. The slab mold is prepared with wooden material (Fig. 3). The circular hollows were prepared by using PVC pipes longitudinal through slabs at one end with hole diameters of 58, 86, and 110 mm. The inner side of the mold has been cleaned and oiled to avoid the adhesion of concrete to the molds. A concrete covering of 20 mm was maintained as a protective layer.



Figure 3: Mold preparation for the layered hollow core slab.

Casting triplet specimens is shown in Fig. 4. The LHCS was cast using the fresh-on-hardened method. The casting was completed in two steps: Firstly, the bottom layer of LWAC was concreted into the mold with a 90 mm thickness. 24hrs later, the upper layer of HSC was concreted and poured into the mold cautiously with a 90 mm thickness. Shear dowels, or bond agent material, are used to connect the two concrete layers of the slab to ensure composite action and better shear transfer. The LWAC surface was cleaned from debris and dust and sprayed with water to obtain the best wet condition before casting the HSC layer. The LWAC layer was covered with plastic sheets directly after casting it for 24 hrs. and then the HSC layer was cast and the LHCS specimens were covered for about 48 hrs before being de-molded and left to cure for 28 days till testing. At a room temperature of around 20-25 °C, the processes of mixing, casting, and curing were prepared. Casting for slab tests is shown in Fig. 5.



Figure 4: Casting triplet specimen for bond strength test.

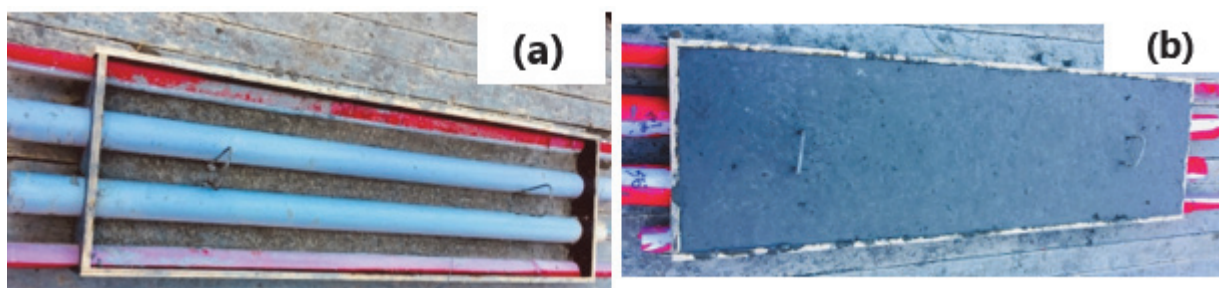


Figure 5: Casting of layered hollow core slabs: (a) after casting of the bottom LWAC layer, (b) after casting of the LHCS after pouring the upper HSC layer.

Test Techniques and instruments

The LHCS samples were tested in flexural under 4-point loading tests with a clear span of 1400mm using a universal hydraulic machine with a capacity of 3000 kN with three different a/d ratios as shown in Fig. 6. The LHCS specimens were cleaned and coated with a white color before testing to inspect the cracks easily. The load was identified by a load cell attached to the machine test, and deflection was indicated using a Linear Variable Distance Transducer (LVDT) fixed at the center of the bottom mid-span slabs. As shown in Fig. 7, strain gages were fixed to determine strain in concrete and longitudinal reinforcement bars. A data logger system linked to a computer was used to obtain the output data for the measuring instruments at all steps of loading. A camera with high pixels was fixed to investigate a crack with the time. The failure load was recorded when the slab showed a decrease in load with a large increase in deflection. The test set up for LHCS slabs is shown in Fig. 8.

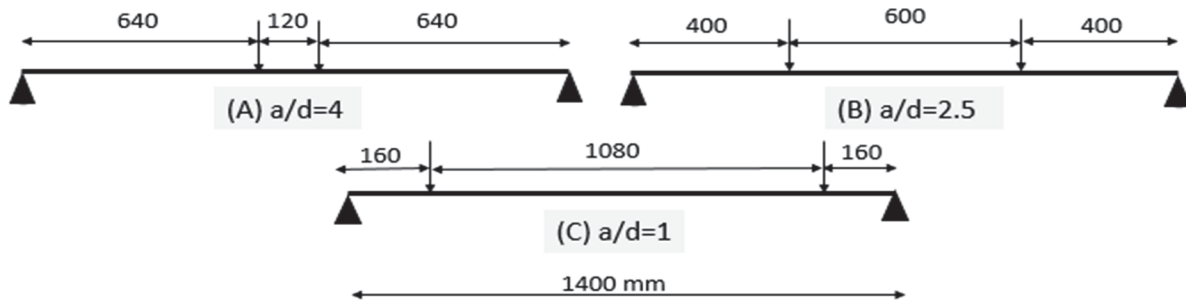


Figure 6: Spans with a/d values.

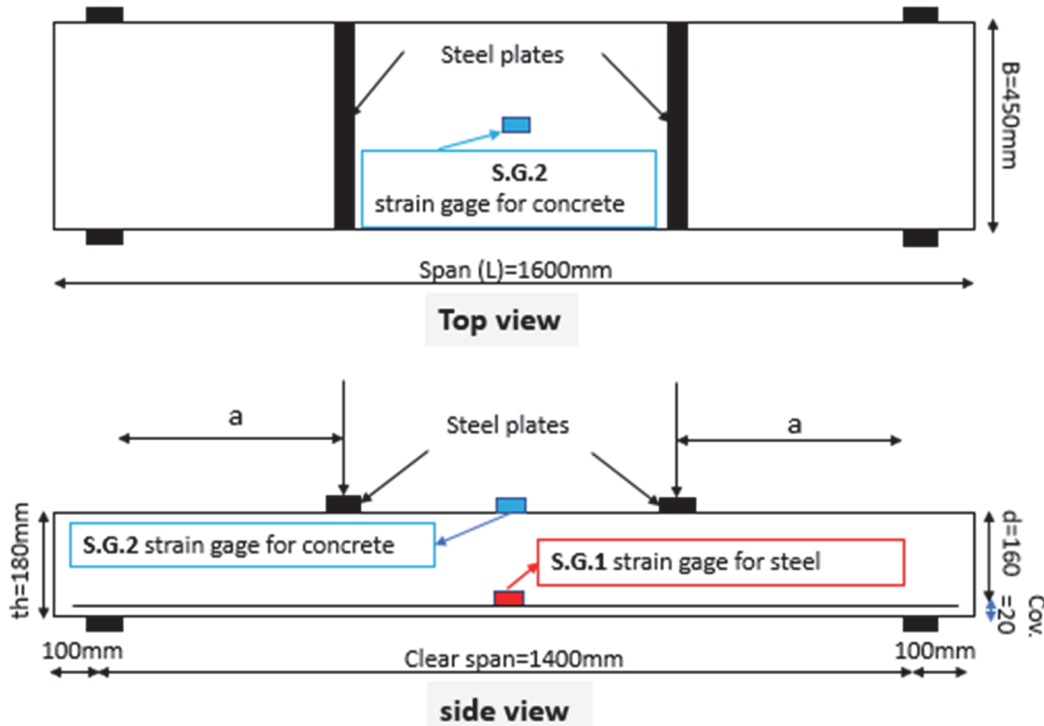


Figure 7: Location of used strain gages at Concrete and Steel.

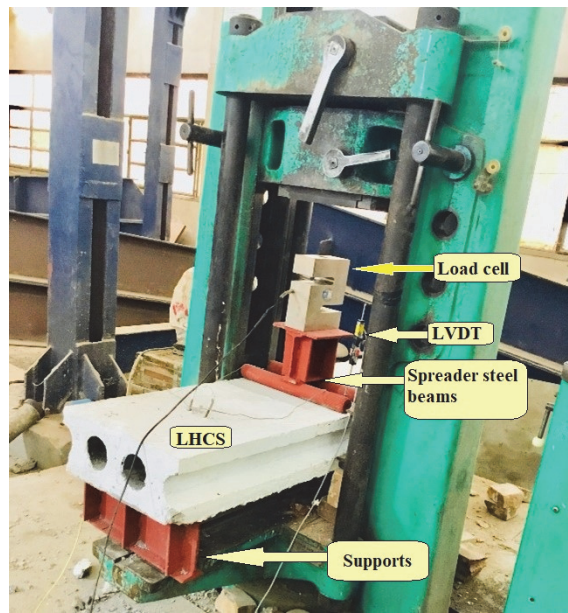


Figure 8: Layered hollow core slab set-up.

EXPERIMENTAL RESULTS

Test of hardened concrete

For push-out tests, triplet specimens without any connection method have the lowest shear bond strength of less than 1 MPa, so it isn't a suitable way to connect the two layers of the tested slabs, while triplet specimens with bond agent material failed with a crack that went through the bond agent material without any damage to particles. The triplet specimens with shear dowels gave a peak shear bond strength value of more than 1 MPa and there was good contact at the interface without any particle damage, so the bond agent material and shear dowel connection methods can be used to connect the two layers of the tested slabs. Test results for push-out tests are given in Tab. 6, and the mode of failure is shown in Fig. 9.

Conn. method	Bond strength (MPa)
without	.837
Bond agent	1.665
Shear dowels	1.727

Table 6: Push-out test results.



Figure 9: Mode of failure for push out test specimens; (a) triplets without connection method, (b) triplets with bond agent material, and (c) triplets with shear dowels.

Test of layered hollow core slabs

The LHCS is positioned in the testing machine as a simple beam supported by a 1400 mm clear span. The load was applied with 5 kN for every step, with recorded the deflection value. The compression and tensile strain values were recorded up to slab failure. There weren't any apparent cracks in the early stages. First cracking load (P_{cr}) and deflection at cracking load (Δ_{cr}) were recorded when the first crack appeared at mid span with increasing applied load. Several cracks were observed and became faster and more spacious with increasing load until specimen failure at ultimate load (P_u) and the deflection at ultimate load (Δ_u) was recorded as following in Tab. 7.

Slab no.	LHCS 1	LHCS 2	LHCS 3	LHCS 4	LHCS 5	LHCS 6	LHCS 7	LHCS 8	LHCS 9
P_u (kN)	34.013	26.051	37.863	23.877	36.754	61.667	36.485	63.375	36.087
P_{cr} (kN)	8.860	6.016	8.943	7.787	10.240	35.240	15.049	39.230	12.642
Δ_u (mm)	4.551	2.643	6.220	3.292	7.169	1.206	2.123	1.673	9.058
Δ_{cr} (mm)	0.425	0.219	0.710	0.342	0.742	0.179	0.340	0.242	0.571
$\Psi = \Delta_u / \Delta_{cr}$	10.707	12.069	8.760	9.626	9.662	6.737	6.245	6.912	15.863
P_{cr}/P_u	0.260	0.231	0.236	0.326	0.279	0.571	0.412	0.619	0.350
Mode of failure	Flex.	Flex.	Flex.	Flex.	Flex.	Sh.	Flex. Sh.	Sh.	Flex.

Table 7: Experimental results for all specimens.

Ultimate and first cracking load

Based on the data in Tab. 7, it was determined that as the (a/d) ratio decreases, the cracking and ultimate load increase. When a/d was reduced from 4 to 1, the first cracking and ultimate loads for LHCS6 increased by 297.74% and 81.30%, respectively, when compared to the control specimen LHCS1. As a/d decreased from 4 to 2.5, the increase in first cracking and ultimate loads for LHCS7 was 69.85% and 7.26%, respectively, compared to control specimen LHCS1. Reducing the applied moment may be the cause of that. It can be noted that the ultimate and cracking loads decreased with increasing %core. The cracking and ultimate load of LHCS3 with %core= 9.785% increases by about 1% and 11.32%, while the cracking and ultimate load of LHCS2 with %core= 35.2% decreases by about 32.1% and 23.40% relative to the reference LHCS1 with %core= 21.5. Reducing loads with increasing %core may be due to decreasing the weight and the volume of concrete in tension zone, where the moment of inertia (E) and the flexural stiffness (EI) of the section are reduced with increasing %core of the LHCS. It was noted that the cracking and maximum load increased with an increase in the bottom RFT ratio. The cracking and ultimate load of LHCS4 reinforced with 3Φ10 are decreased by about 12.11% and 29.8%, while for LHCS5 reinforced with 3Φ16 is increased by about 15.57% and 8.05% compared to slab LHCS1 with reinforcement of 3Φ12. This could be due to increased stress. Using shear dowels leads to a direct increase in the load carrying capacity, which increases the flexural resistance of LHCS8 with a/d= 1 and LHCS9 with a/d= 4. The cracking load of LHCS9 increased by approximately 42.68% to 12.642 kN, and the failure load increased by approximately 6.11% to 36.087 kN when compared to LHCS1, which used bond agent material and was tested with a/d =4. The cracking load of LHCS8 increased to reach 39.23 kN with an increase of about 11.32%, and the increase in failure load was about 2.77% as the failure load reached 63.375 kN compared to LHCS6 that used bond agent material and tested with a/d=1. The increase in applied load of LHCS8 and LHCS9 with shear dowels is due to good contact between the two concrete layers of the slab, which avoids horizontal sliding and enhances the shear strength.

Deflection at first cracking and ultimate load

From the data given in Tab. 7, the reduction in a/d causes a decrease in the mid-span deflection (Δ_u) and a decrease in the deflection at cracking load (Δ_{cr}) of the LHCS. For LHCS6, having a reduction in a/d ratio from 4 to 1 shows a reduction in the ultimate deflection by 73.5% and a decrease in cracking deflection by 57.88% compared to LHCS1. For LHCS7, having a reduction in a/d ratio from 4 to 2.5 shows a reduction in the ultimate deflection by 53.35% and a decrease in cracking deflection compared to LHCS1. It can be concluded that increasing %core with percentages of 35.2% of LHCS2 decreases the ultimate deflection and cracking deflection by 41.92% and 48.47%, respectively, when compared with LHCS1, while decreasing %core with percentages of 9.785% of LHCS3 increases the ultimate deflection by 36.67% and increases the cracking deflection by 67.05% when compared with LHCS1. It was noted that the ultimate and cracking deflection of LHCS4 reinforced with 3Φ10 is decreased by about 27.66% and 19.53%, respectively, compared to LHCS1 with reinforcement of 3Φ12, while the ultimate and cracking deflection of LHCS5 reinforced with 3Φ16 is increased by about 57.52% and 74.58%, respectively, compared to LHCS1 with reinforcement of 3Φ12. Using shear dowels causes an increase



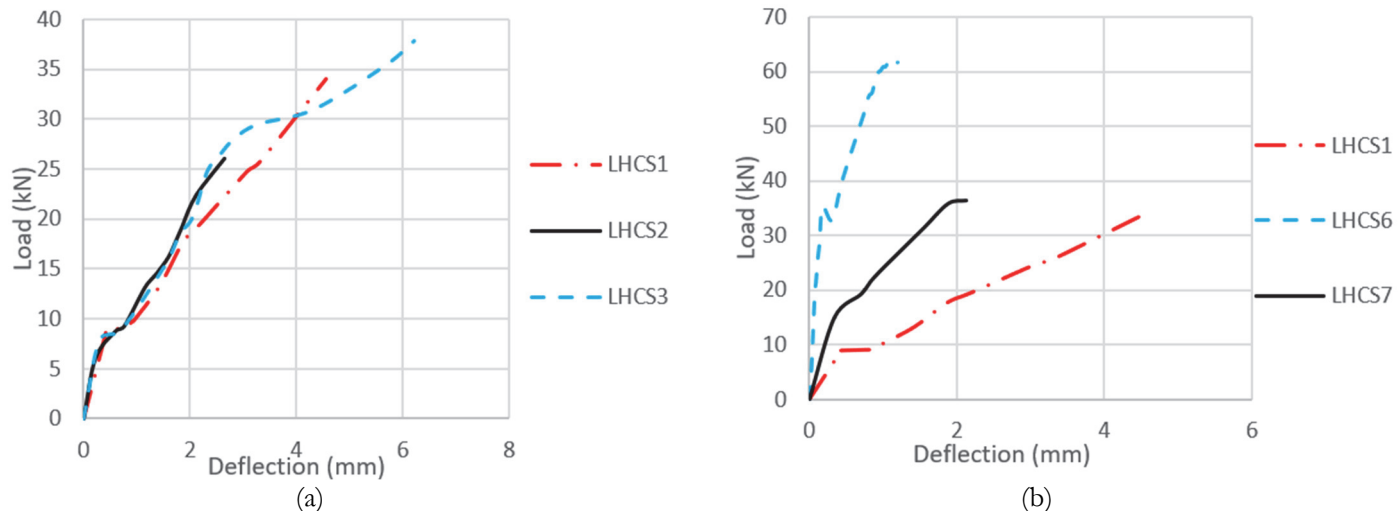
in cracking and ultimate deflection for specimens compared to specimens that use bond agent material to connect the two layers of the slab. The ultimate and cracking deflection of LHCS8 increased to reach 1.673 mm and .242 mm with an increase of about 38.72% and 35.19%, respectively, compared to LHCS6, which used bond agent material to connect the two concrete layers of the slab and tested with $a/d = 1$. The ultimate and cracking deflections of LHCS9 increased by about 99.03% and 34.35%, respectively, when compared to LHCS1, which used bond agent material to connect the two layers of the slab and was tested with $a/d = 4$.

Ductility ratio

The ductility ratio (the deflection at ultimate load to the deflection at first crack load $\Psi = \Delta u/\Delta c_r$) was investigated. Increasing the ductility ratio means increasing the ability of the slab to bear more deflection before failure. From the data given in Tab. 7, it can be noted that the ductility ratio varies from 6.245 to 15.863, which means good ductility performance. The ductility ratio decreased with decreasing a/d . The ductility ratio for LHCS6, and LHCS7 with $a/d = 1$, and $a/d = 2.5$ decreased by 37.07% and 41.67%, respectively, relative to LHCS1 with $a/d = 4$. The ductility ratio of LHCS3 with a %core= 9.785% is decreased by 18.18% relative to LHCS1 with a %core= 21.5%. The percentage of increase of LHCS2 with a %core= 35.2% is 12.72% relative to LHCS1 with a %core= 21.5%. The ductility ratio for LHCS 4 reinforced with 3Φ10 reduced by 10.1%, and for LHCS 5 reinforced with 3Φ16 decreased by 9.76%, compared to the control slab reinforced by 3Φ12. The ductility ratio for LHCS8 and LHCS9 with shear dowels increased by 2.6% and 48.15%, respectively, compared to LHCS6 and LHCS1 with bond agent material.

Load deflection curves

From the load-deflection relations of the LHCS, which are given in Fig. 10, it displays three stages in the load-deflection curve in general as follows: The first stage is the un-cracked stage (elastic), where there was a linear increase in deflection with loading until the appearance of the first crack. The second stage (pseudo-elastic stage), where there was an insignificant difference in the slope after the first crack, the third stage (plastic stage), where there was a rapid increase in deflection with a slight increase in loading till the failure of the slab. Increasing the ratio of a/d increases the deflection determined at any loading stage. The control slab showed a typical under-reinforced performance. The first flexural crack was observed exactly below the load point when the load reached 8.86 kN. After yielding of R_f , the load deflection curve flattened after reaching a peak load of 34.013 kN. The load deflection relation of a specimen with shear dowels at the interface, which achieved good composite action between the two layers, was found to be stiffer than the control slab, which was connected with bond agent material. It is obvious that all slabs with an a/d ratio of 4 have similar general behavior, with a smaller difference in the value of maximum deflection. For a/d ratios of 1 and 2.5, display is unlike performance because the mode of failure is different.



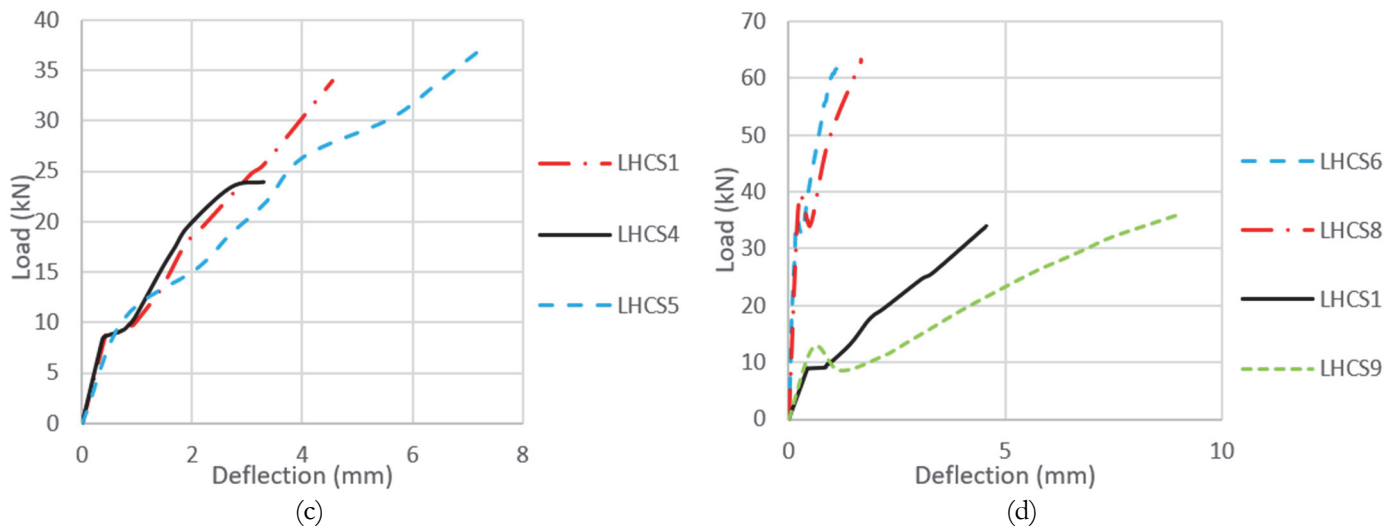
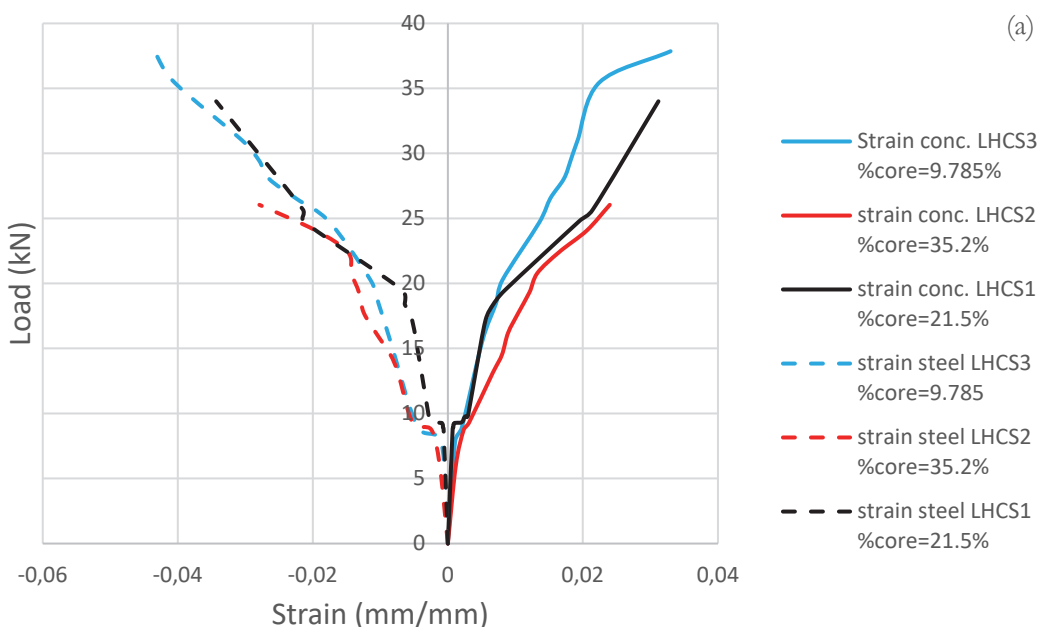
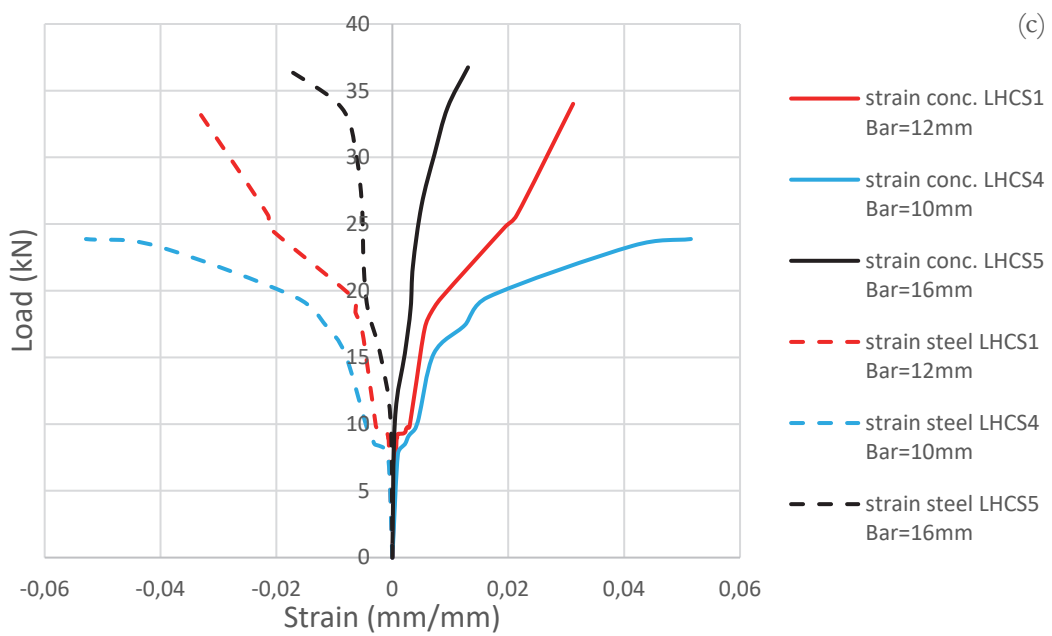
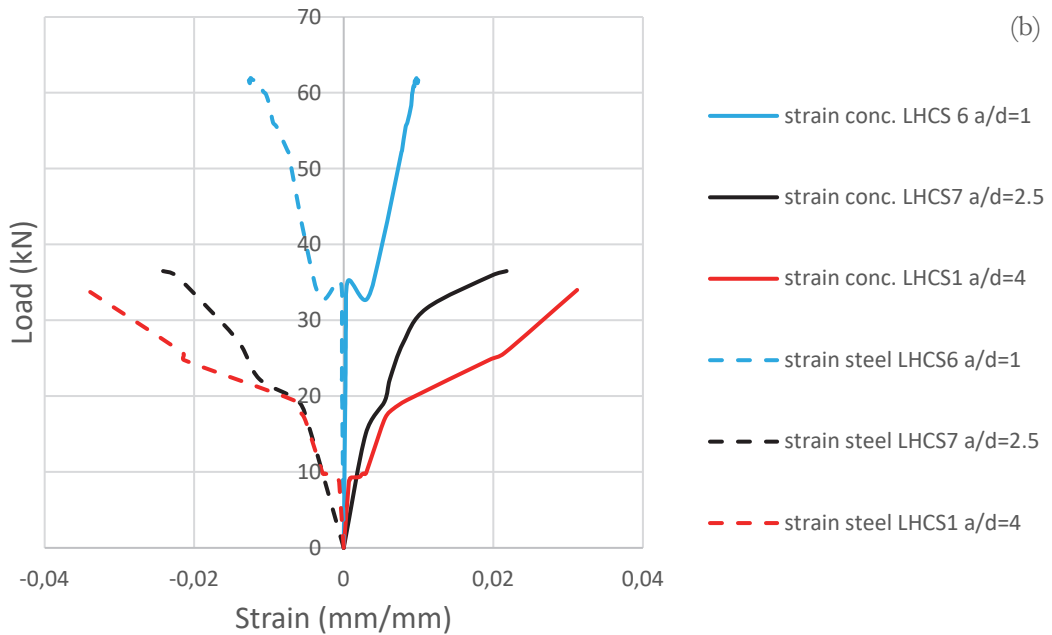


Figure 10: the load-deflection curve of the layered hollow core slabs: (a) Effect of %core variation, (b) Effect of a/d variation, (c) Effect of RFT variation, and (d) Effect of connection method variation.

Strain load diagram

The strain load diagrams obtained from the strains were fixed on the top surface of the concrete at the compression zone and in the bottom middle of the intermediate main steel RFT at the tension zone (Fig. 11). It is clear that the strain increases with the applied load linearly at a slight rate till observing the first crack, then the strain increases with the applied load at a faster rate until failure. Reducing %core leads to increasing the concrete strain due to enhanced stiffness and leads to increasing the steel strain due to increasing ultimate strength. For LHCS1 tested with $a/d = 4$, the strain was insignificant till the occurrence of the first crack at an applied load of 8.86 kN, and with further loading, the RFT yielded and then reached its ultimate strain at .038 mm/mm. For LHCS6 tested with $a/d=1$, the whole load has been taken by the concrete only in the first loading stage of pre-cracking. After increasing load, the concrete began to crack and RFT had more strain linearly with the load till it reached its peak value of .0127 mm/mm. When RFT reached its maximum strain of .024 mm/mm for LHCS7 tested with $a/d = 2.5$, the primary stiffness increased and the slab collapsed. LHCS8 and LHCS9 tested with shear dowels showed very stiff behavior and collapsed before the RFT reached its yield value due to the active influence of shear dowels. The strain in the RFT reached its peak value of .0168 mm/mm at slab failure. For LHCS5, increasing the RFT ratio causes a decrease in the strain value. LHCS4 showed an increase in strain due to decreasing the RFT ratio.





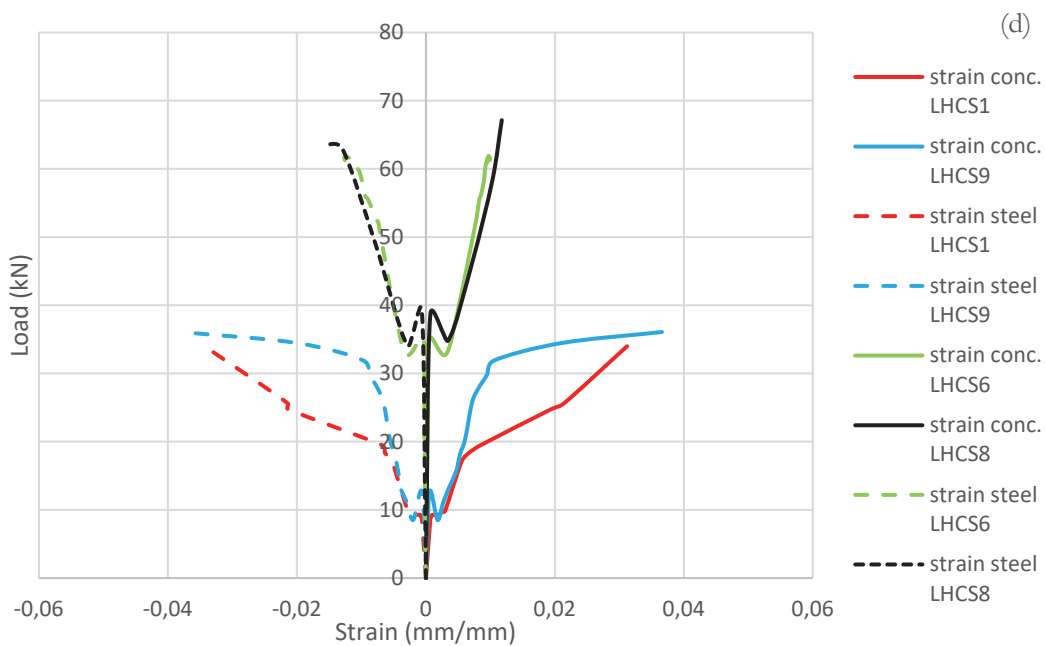


Figure 11: Strain load diagrams for LHCS: (a) Effect of %core variation, (b) Effect of a/d variation, (c) Effect of RFT variation, and (d) Effect of connection method variation.

Mode of failure

Three different modes of failure have been investigated. The position of the applied loading (a/d ratio) is assumed to be the main factor that affects the mode shape. All specimens with $a/d = 4$ collapsed in flexural, all specimens with $a/d = 2.5$ collapsed in flexural shear, and all specimens with $a/d = 1$ collapsed in shear, and they are as follows:

Flexural failure: The failure occurs when the tensile stress increases the tensile strength, as the failure starts with an initial vertical crack, which decreases the compression zone depth. The steel area in LHCS is often small, so the slab exhibits a ductile failure. For control specimen LHCS1, the first flexural crack was observed at 8.86 kN (26.05% of the ultimate load) at the mid-span of the slab, and after increasing the applied load, the number of cracks increased and extended toward the compression zone and became wider. Another flexural crack was observed between line loads and supports. The cracks then extended inclinedly toward the loading points. Finally, the LHCS1 collapsed in flexure at a load of 34.013 kN.

Flexural shear failure: This failure occurred when the flexural cracks were increased in the shear span through the early stages of loading and, with increasing applied loading, these cracks propagated toward the load line in a diagonal direction. For LHCS7 tested with $a/d = 2.5$, it exhibits similar behavior as LHCS1 through the early stages of loading. The first crack appeared at an applied load of 15.049 kN and, with increasing load, the flexural cracks in the shear span became faster than the flexural cracks between the two-line loads. Then, they inclined and propagated towards the loading lines with a crack angle of about 40° and the slab finally collapsed at 36.485 kN.

Shear failure: This failure occurs when the principal tensile stress caused by flexure and shear exceeds the tensile strength. The first crack formed below the point of loading exactly and more cracks occurred with increasing loads and the flexural crack extended toward the supports and converted to shear crack and the slab failed. For LHCS6 tested with $a/d = 1$, the initial crack appeared at a load of 35.24 kN (57.14% of the ultimate load) at the shear span region near supports and with increasing loading, cracks extended towards the supports and finally failed at a load of 61.667 kN with a crack angle of 50° approximately. The crack angle increases as the a/d ratio decreases.

VERIFICATION STUDY

The experimental program was compared with the finite element models (FEM) to confirm the validity of the model analysis as shown in Fig. 12. A comparison between the experimental and numerical load-deflection curves showed a very good correlation between them for all loading stages (Fig. 13). The FEM was able to predict the ultimate failure load of the layered hollow core slab specimens, and it can be used to simulate the experimental program using



ANSYS software. SOLID65 (a 3D finite element with eight nodes) having three degrees of freedom at each node in x, y, and z directions was used to simulate the used LWAC and HSC concretes. LINK 180 (a 3-D spar element) with three degrees of freedom at each node in x, y, and z directions was used to simulate steel reinforcement bars. SOLID185(a 3D finite element with eight nodes) having three degrees of freedom at each node in x, y, and z directions was used to simulate the steel plates at supports and loading points [45]. The properties of used concrete, plates, and steel are given in Tab. 8. Three different mesh sizes of 50, 20, and 10 mm were chosen to study the convergence. From the convergence study, an optimum mesh size of 20 mm was selected for LHCS models so that each couple of various materials could share a similar node between them to obtain accurate results.

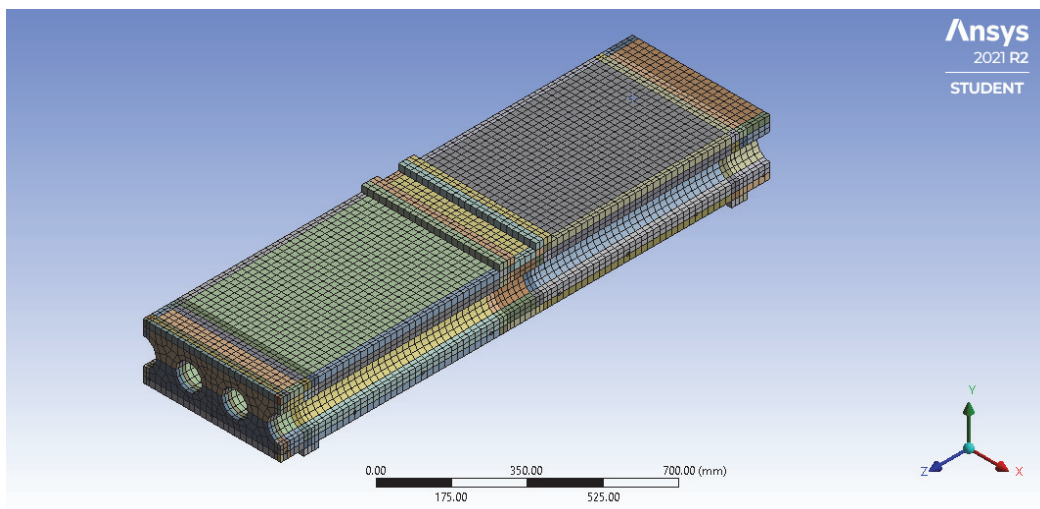
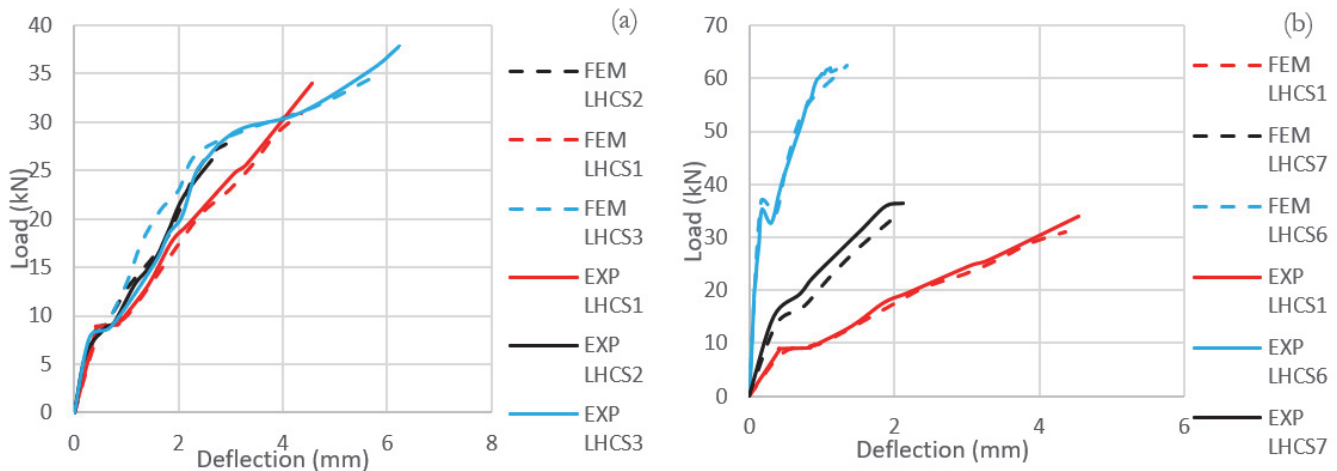


Figure 12: Sample representation of developed FE models.

Material	Elastic modulus (MPa)	Poisson's ratio	Compressive strength (MPa)	Yield strength (MPa)	Tensile strength (MPa)
HSC	58593.75	.25	62.5	-	4.53
LWAC	20437.5	.25	21.8	-	1.28
Non-linear steel	200000	.2	-	525	-
Linear steel	200000	.3	-	-	-

Table 8: Properties of used concrete, plates, and steel.



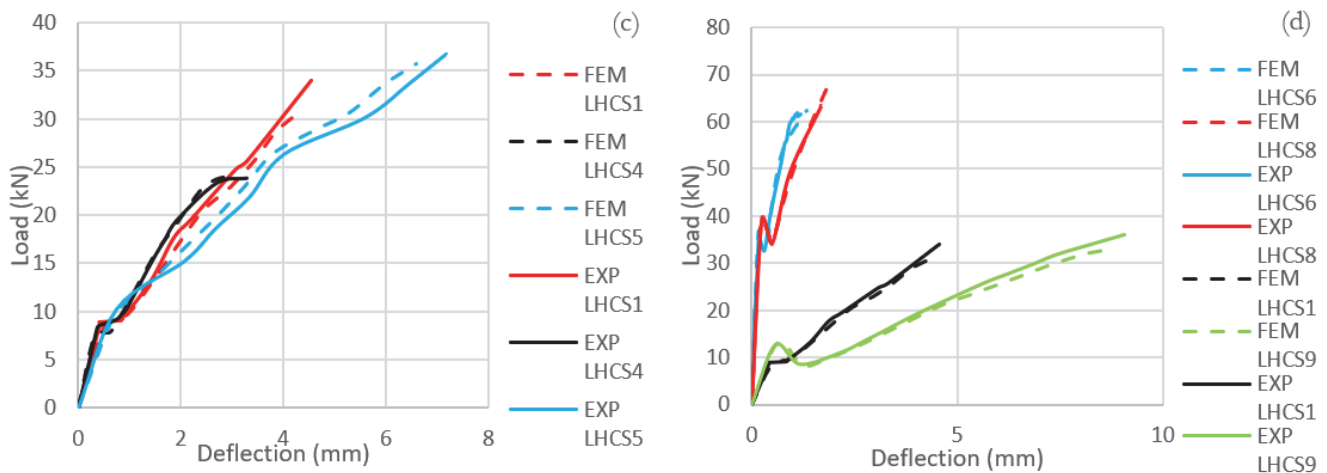


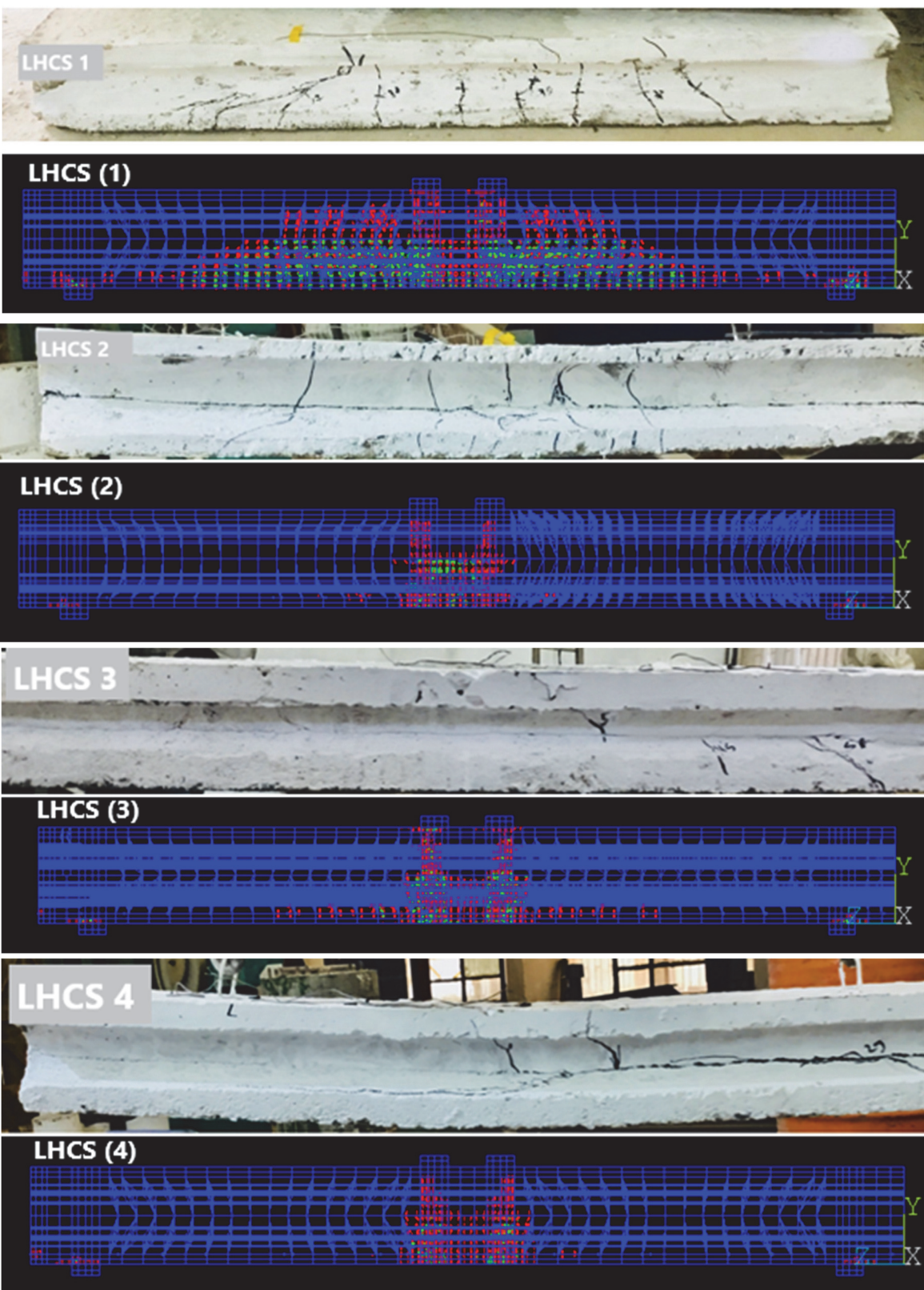
Figure 13: Validation load-deflection curve (a) effect of %core variation, (b) effect of a/d variation, (c) effect of RFT variation, (d) effect of connection method variation.

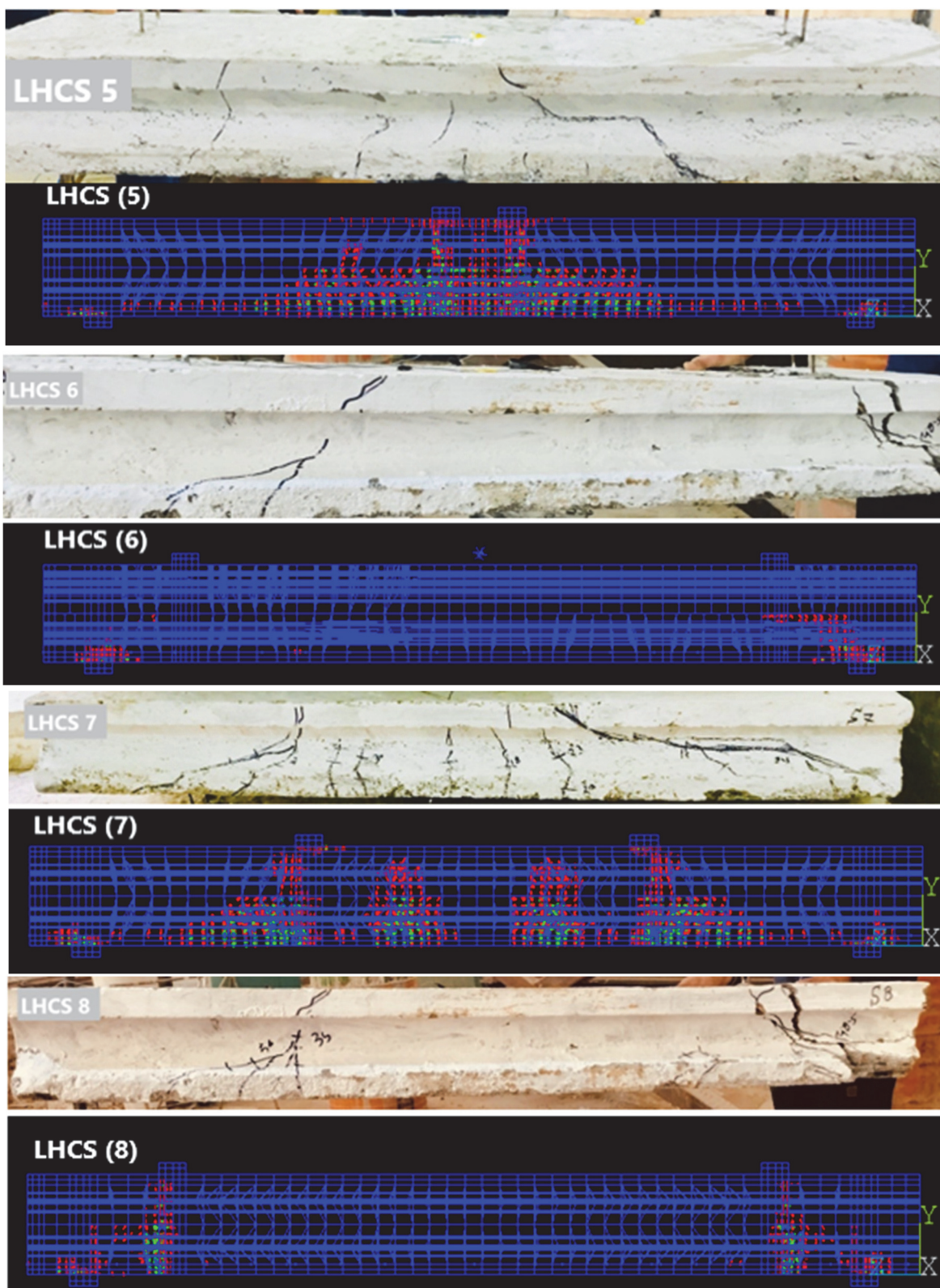
Comparison between experimental and numerical results.

Tab. 9 explains the comparison between numerical and experimental results attained for all studied slabs and reveals that the analytical method summarized here can be used to simulate LHCS behavior in an acceptable way when there is no material difference. The numerical results were accepted with the experimental results with a difference of less than 10 %. The failure load for the FEM is the last applied load before the starting divergence of the program due to the several cracks. The deflection at ultimate load is the vertical displacement in Y-direction (UY) at the mid-span of the slab for the FEM. Crushing or cracking in concrete elements is illustrated in the ANSYS program by displaying circles at the location. Fig. 14 shows the comparison of numerical and experimental cracking patterns for all the layered hollow-core slabs. The FEM also predicted similar failure modes.

	Slab no.	LHCS 1	LHCS 2	LHCS 3	LHCS 4	LHCS 5	LHCS 6	LHCS 7	LHCS 8	LHCS 9
Pcr (kN)	Exp.	8.86	6.016	8.943	7.787	10.24	35.24	15.049	39.23	12.642
	FEM	8.17	5.884	9.6	7.542	9.332	36.739	13.683	38.772	13.11
	Exp./FEM	1.084	1.023	0.932	1.032	1.097	0.959	1.100	1.011	0.964
Pu (kN)	Exp.	34.013	26.051	37.863	23.877	36.754	61.667	36.485	63.375	36.087
	FEM	30.929	27.834	34.547	24.070	35.728	62.473	33.130	67.153	32.900
	Exp./FEM	1.100	0.936	1.096	0.992	1.029	0.987	1.101	0.944	1.097
Δ_{cr} (mm)	Exp.	0.425	0.219	0.710	0.342	0.742	0.179	0.340	0.242	0.571
	FEM	0.470	0.243	0.652	0.316	0.675	0.163	0.378	0.220	0.635
	Exp./FEM	0.904	0.903	1.089	1.082	1.099	1.098	0.900	1.099	0.900
Δu (mm)	Exp.	4.551	2.643	6.220	3.292	7.169	1.206	2.123	1.673	9.058
	FEM	4.355	2.937	5.670	3.063	6.593	1.339	1.937	1.818	8.808
	Exp./FEM	1.045	0.900	1.097	1.075	1.087	0.901	1.096	0.920	1.028
Pcr/Pu	Exp.	0.260	0.231	0.236	0.326	0.279	0.571	0.412	0.619	0.350
	FEM	0.264	0.211	0.278	0.313	0.261	0.588	0.413	0.577	0.398
$\Delta u/\Delta_{cr}$	Exp.	10.707	12.069	8.760	9.626	9.662	6.737	6.245	6.912	15.863
	FEM	9.265	12.105	8.696	9.687	9.762	8.212	5.126	8.260	13.881

Table 9: Experimental and numerical results for all specimens.





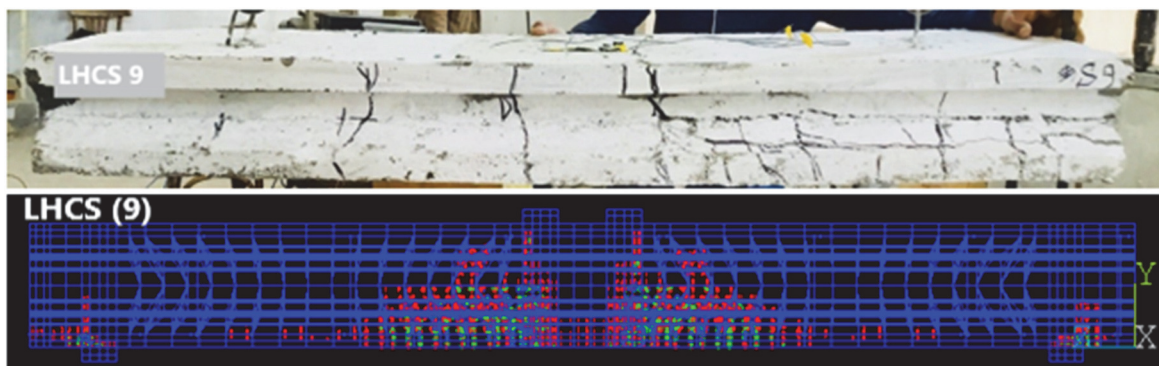


Figure 14: Experimental and numerical crack patterns for (LHCS 1: LHCS9).

CONCLUSIONS

From the previous analysis of all FE models for LHCSS, the experimental results, and their analytical simulation, the specific conclusions that can be drawn from this study are as follows:

- Experimental and theoretical capacities fit well with each other.
- The Layered Hollow Core Slab system can be used to obtain a slab with an optimum weight-to-strength ratio.
- The experimental mid-span deflection versus load curve of flexural testing coincides well with the corresponding theoretical curve.
- With decreasing (a/d) ratio, the cracking load and ultimate load will increase. The reduction in the a/d values leads to a decrease in the maximum deflection in the mid-span (Δ_u) and a decrease in the deflection at the first cracking load (Δ_{cr}) of the layered hollow core slabs due to a decrease in applied moment.
- The ultimate and first cracking loads decreased with increasing %core. The ultimate and cracking deflection decreased due to decreasing the moment of inertia (E) of the section. Therefore, the flexural stiffness (EI) will decrease with increasing the diameter of longitudinal voids in LHSC specimens.
- In this study, the optimum slab was one with a core value of 21.5% in order to preserve ultimate strength while also meeting economic requirements.
- Using shear dowels leads to a direct increase in load carrying capacity and consequently, an increase in the flexural resistance of the slab and leads to an increase in deflection at first cracking load and deflection at ultimate load compared to a specimen that uses bond agent material to connect the two layers of the LHCS.
- Shear dowels ensure an efficient bond between the two concrete layers, preventing horizontal sliding and increasing the shear resistance of the LHCS.
- The first cracking load value and ultimate load value increased with an increase in bottom reinforcement values. The deflection at ultimate load and the deflection at first cracking load is increased for the layered hollow core slabs due to the increase in stresses.
- Reduced in %core causes an increase in strains in the compression zone due to increased LHCS stiffening and an increase in strains in the tension zone due to increased LHCS ultimate strength.
- All specimens with $a/d = 4$ collapsed in flexural, all specimens with $a/d = 2.5$ collapsed in flexural shear, and all specimens with $a/d = 1$ collapsed in shear due to the position of applied loads.

REFERENCES

- [1] Monisha, K.M., Srinivasan, G. (2017). Experimental Behaviour of Prestress Hollow Core Slab , Rc Hollow Core Slab and Normal Rc Solid Slab, Int. J. Eng. Tech. Res., 4(4), pp. 1090–3.
- [2] Nassif Sabr, Y., Husain Khalaf Jarallah, D., Hassan Issa Abdul Kareem, D. (2018). Improving the Shear Strength of Lightweight RC Thick Hollow Core Slab Made of Recycled Materials, Int. J. Eng. Technol., 7(4.20), pp. 403, DOI: 10.14419/ijet.v7i4.20.26143.
- [3] Mhalhal, J.M. (2017). Prestressed Precast Hollow-Core Slabs with Different Shear Span to Effective Depth Ratio, Wasit



- J. Eng. Sci., 5(2), pp. 1–11, DOI: 10.31185/ejuow.vol5.iss2.53.
- [4] Al-Azzawi, A.A., Abed, S.A. (2017). Investigation of the behavior of reinforced concrete hollow-core thick slabs, *Comput. Concr.*, 19(5), pp. 567–577, DOI: 10.12989/cac.2017.19.5.567.
- [5] Al-Shaarba, I.A., Al-Azzawi, A.A., Abdulsattar, R. (2018). A state of the art review on hollow core slabs, *ARPN J. Eng. Appl. Sci.*, 13(9), pp. 3240–5.
- [6] Hussein, Z.M., Ismail Khalil, W., Khalid Ahmed, H. (2018). Structural behavior of sustainable hollow core slabs reinforced with hybrid fibers, *Journal of Engineering and Applied Sciences*, 13(24), pp. 9328–9334.
- [7] Prakashan, L.V., George, J., Edayadiyil, J.B., George, J.M. (2016). Experimental Study on the Flexural Behavior of Hollow Core Concrete Slabs, *Appl. Mech. Mater.*, 857, pp. 107–112, DOI: 10.4028/www.scientific.net/amm.857.107.
- [8] Li, S., Song, C. (2019). Mechanical performance test and analysis of prestressed lightweight aggregate concrete hollow slab, *Adv. Struct. Eng.*, 22(8), pp. 1830–1844, DOI: 10.1177/1369433219825998.
- [9] Gul, A., Shahzada, K., Alam, B., Badrashi, Y.I., Khan, S.W., Khan, F.A., Ali, A., Rehman, Z.U. (2020). Experimental study on the structural behavior of cast in-situ hollow core concrete slabs, *Civ. Eng. J.*, 6(10), pp. 1983–91, DOI: 10.28991/cej-2020-03091597.
- [10] Abed, A.A.A.-A. and S.A. (2016). Numerical analysis of reinforced concrete hollow-core slabs, *ARPN Jour Nal Eng. Ing Appl. Sci.*, 11(181 9-66 08), pp. 15.
- [11] Mohamed, M.S., Thamboo, J.A., Jeyakaran, T. (2020). Experimental and numerical assessment of the flexural behaviour of semi-precast-reinforced concrete slabs, *Adv. Struct. Eng.*, 23(9), pp. 1865–1879, DOI: 10.1177/1369433220904011.
- [12] Baran, E. (2015). Effects of cast-in-place concrete topping on flexural response of precast concrete hollow-core slabs, *Eng. Struct.*, 98, pp. 109–117, DOI: 10.1016/j.engstruct.2015.04.017.
- [13] Masénas, J., Šalna, R., Juknevičius, L., Valivonis, J. (2021). Deflection analysis of layered slabs with plastic inserts, *Materials (Basel)*, 14(20), DOI: 10.3390/ma14206050.
- [14] Kankeri, P., Suriya Prakash, S., Pachalla, S.K.S. (2018). Experimental and Numerical Studies on Efficiency of Hybrid Overlay and Near Surface Mounted FRP Strengthening of Pre-cracked Hollow Core Slabs, *Structures*, 15, pp. 1–12, DOI: 10.1016/j.istruc.2018.05.003.
- [15] Nabil, A., Meleka, N., Heiza, K. (2017). Effects of Different Types of Concrete Toppings on the Behavior of Pphc Slabs, *ERJ. Eng. Res. J.*, 40(4), pp. 331–339, DOI: 10.21608/erjm.2017.66359.
- [16] Torelli, G., Fernández, M.G., Lees, J.M. (2020). Functionally graded concrete: Design objectives, production techniques and analysis methods for layered and continuously graded elements, *Constr. Build. Mater.*, 242, DOI: 10.1016/j.conbuildmat.2020.118040.
- [17] Balevičius, R., Marciukaitis, G. (2013). Linear and Non-linear Creep models for a multi-layered concrete composite, *Arch. Civ. Mech. Eng.*, 13(4), pp. 472–490, DOI: 10.1016/j.acme.2013.04.002.
- [18] Marciukaitis, G., Juknevicius, L. (2010). Influence of the initial state of stress and strain on the cracking of shear section of layered reinforced concrete structures, 10th Int. Conf. Mod. Build. Mater. Struct. Tech., , pp. 713–9.
- [19] Pratama, M.M.A., Suhud, R.K., Puspitasari, P., Kusuma, F.I., Rahma Putra, A.B.N. (2019). Finite element analysis of the bending moment-curvature of the double-layered graded concrete beam, *IOP Conf. Ser. Mater. Sci. Eng.*, 494(1), DOI: 10.1088/1757-899X/494/1/012064.
- [20] Brault, A., Lees, J.M. (2020). Wet casting of multiple mix horizontally layered concrete elements, *Constr. Build. Mater.*, 247, DOI: 10.1016/j.conbuildmat.2020.118514.
- [21] AL-Farttoosi, H.K.A., Hussain, H.K., Abdulrazzaq, O.A. (2021). Flexural behavior of two-layer beams made with normal and lightweight concrete layers, *Period. Eng. Nat. Sci.*, 9(2), pp. 1124–1140, DOI: 10.21533/pen.v9i2.1952.
- [22] Pratama, M.M.A., Aylie, H., Gan, B.S., Umniati, B.S., Risdanaren, P., Fauziyah, S. (2017). Effect of concrete strength gradation to the compressive strength of graded concrete, a numerical approach, *AIP Conf. Proc.*, 1887, DOI: 10.1063/1.5003512.
- [23] Gan, B.S., Aylie, H., Pratama, M.M.A. (2015). The behavior of graded concrete, an experimental study, *Procedia Eng.*, 125, pp. 885–891, DOI: 10.1016/j.proeng.2015.11.076.
- [24] Pratama, M.M.A. (2016). An Experimental Study and Finite Element Approach to the Behavior of Graded Concrete, Thesis Master of Engineering at the Faculty, DOI: 10.13140/RG.2.1.4082.4568.
- [25] Abdillah Pratama, M.M., Umniati, B.S., Arumsari Mutiara Wulandari, B., Han, A.L., Sthenly Gan, B., Zhabrinna, Z. (2018). Modulus elasticity of the graded concrete, a preliminary research, *MATEC Web Conf.*, 195, pp. 1–8, DOI: 10.1051/matecconf/201819501005.
- [26] Sulistyana., Purwanto., Widoanindyawatib, V., Pratama, M.M.A. (2014). The influence of compression applied during production to the compression strength of dry concrete: An experimental study., *Procedia Eng.*, 95(Scescm), pp. 465–72, DOI: 10.1016/j.proeng.2014.12.206.



- [27] Nes, L.G., Øverli, J.A. (2016). Structural behaviour of layered beams with fibre-reinforced LWAC and normal density concrete, *Mater. Struct.*, 49(1–2), pp. 689–703, DOI: 10.1617/s11527-015-0530-9.
- [28] Korol, E.A., Tho, V.D. (2020). Bond strength between concrete layers of three-layer concrete structures, *IOP Conf. Ser. Mater. Sci. Eng.*, 775(1), DOI: 10.1088/1757-899X/775/1/012115.
- [29] Farzad, M., Shafieifar, M., Azizinamini, A. (2019). Experimental and numerical study on bond strength between conventional concrete and Ultra High-Performance Concrete (UHPC), *Eng. Struct.*, 186(December 2018), pp. 297–305, DOI: 10.1016/j.engstruct.2019.02.030.
- [30] Said, A., Elsayed, M., El-Azim, A.A., Althoe, F., Tayeh, B.A. (2022). Using ultra-high performance fiber reinforced concrete in improvement shear strength of reinforced concrete beams, *Case Stud. Constr. Mater.*, 16, pp. e01009, DOI: 10.1016/j.cscm.2022.e01009.
- [31] Sajedi, F., Razak, H.A. (2011). Comparison of different methods for activation of ordinary Portland cement-slag mortars, *Constr. Build. Mater.*, 25(1), pp. 30–38, DOI: 10.1016/j.conbuildmat.2010.06.060.
- [32] Li, P.P., Sluijsmans, M.J.C., Brouwers, H.J.H., Yu, Q.L. (2020). Functionally graded ultra-high performance cementitious composite with enhanced impact properties, *Compos. Part B Eng.*, 183, DOI: 10.1016/j.compositesb.2019.107680.
- [33] Smorkalov, D., Zhuravskiy, O., Delyavskyy, M. (2019). Experimental and theoretical studies of single and double-layer slabs supported on four sides, *AIP Conf. Proc.*, 2077, DOI: 10.1063/1.5091913.
- [34] Lapko, A., Sadowska-Buraczewska, B., Tomaszewicz, A.J. (2005). Experimental and numerical analysis of flexural composite beams with partial use of high strength/high performance concrete, *J. Civ. Eng. Manag.*, 11(2), pp. 115–20, DOI: 10.1080/13923730.2005.9636340.
- [35] Li, Q., Xu, S. (2009). Experimental investigation and analysis on flexural performance of functionally graded composite beam crack-controlled by ultrahigh toughness cementitious composites, *Sci. China, Ser. E Technol. Sci.*, 52(6), pp. 1648–1664, DOI: 10.1007/s11431-009-0161-x.
- [36] Zhang, M.-H., Liu, X., Chia, L.-S. (2011). High-Strength High-Performance LightWeight Concrete- A Review, *Proc. 9th Int. Symp. High Perform. Concr.*, pp. 16.
- [37] Santhanam, N., Anbuarasu, G. (2020). Experimental study on high strength concrete (M60) with reused E-waste plastics, *Mater. Today Proc.*, 22, pp. 919–25, DOI: 10.1016/j.matpr.2019.11.107.
- [38] O, G. (2008). High-strength concrete. Developments in the Formulation and Reinforcement of Concrete, Elsevier, pp. 153–70, DOI: 10.1016/C2017-0-03347-5.
- [39] Srinivas, H. R. and Dr. Sadath Ali Khan Zai, (2017), Behaviour of high performance Fibre reinforced concrete layered beams, *International Journal of Current Research*, 9(10), pp. 61245-61250.
- [40] Shafiq, P., Jumaat, M.Z., Mahmud, H. (2010). Mix design and mechanical properties of oil palm shell lightweight aggregate concrete: A review, *Int. J. Phys. Sci.*, 5(14), pp. 2127–34.
- [41] Sayadi AA, Neitzert TR, C.G. (2016). Feasibility of a biopolymer as lightweight aggregate in perlite concrete, *Int. J. Civ. Environ. Eng.*, 10(751–61), pp. 6.
- [42] Heinz P, Herrmann M, Sobek W. (2012). Production method and application of functionally graded components in construction (Herstellungsverfahren und Anwendungsbereiche für funktional gradierte Bauteile im Bauwesen). Stuttgart: Fraunhofer IRB Verlag;
- [43] Husain, M., Khater, M.A., El-ghamry, A. (2018). Enhancement of mechanical properties of lightweight concrete, *International Journal of Engineering & Technology*, 7(4), pp. 4808–13, DOI: 10.14419/ijet.v7i4.17687.
- [44] Addibond-65. Available at: <https://cmpgroup.net/>.
- [45] ANSYS 2018. Available at: <http://www.ansys.com>.